

22 September, 1999

Inelastic diffraction data and the \mathcal{P} omeron trajectory

Samim Erhan¹ and Peter Schlein²

University of California³, Los Angeles, California 90095, USA.

Abstract

We demonstrate that all available inclusive pp and $\bar{p}p$ single diffraction data from ISR to Tevatron require an effective \mathcal{P} omeron trajectory whose intercept, $\alpha(0)$, changes with energy; it decreases from 1.10 at low energy to about 1.03 at the SPS and perhaps smaller at the Tevatron. This result, when combined with a relatively s -independent trajectory, $\alpha(t) \sim 0.92 - 0.95$ in the range, $1.0 < |t| < 1.5$ GeV 2 , specifies a new effective \mathcal{P} omeron trajectory in inelastic diffraction.

submitted to Physics Letters B

¹samim.erhan@cern.ch

²peter.schlein@cern.ch

³Supported by U.S. National Science Foundation Grant PHY94-23142

1 Introduction

Single diffraction, or the inclusive inelastic production of beam-like particles with momenta within a few percent of the associated incident beam momentum, as in:

$$p(\bar{p}) + p_i \rightarrow X + p_f \quad (1)$$

has been studied for more than 30 years. The chief characteristic of data from these processes is the existence of a pronounced enhancement at Feynman- x_p of p_f near unity, which is interpreted using Regge phenomenology[1–6] as evidence for the dominance of \mathcal{P} omeron-exchange (see Fig. 1). The observed x_p spectrum reflects the distribution of the exchanged \mathcal{P} omeron's momentum fraction in the proton⁴, $\xi \equiv x_{\mathcal{P}} = 1 - x_p$, and momentum transfer, t .

A relatively recent idea[7, 8, 9] underlying the phenomenology is that, although the \mathcal{P} omeron's existence in the proton is due to non-perturbative QCD, once the \mathcal{P} omeron exists, perturbative QCD processes can occur in proton- \mathcal{P} omeron and γ^* - \mathcal{P} omeron interactions. Ref. [7] proposed the study of such hard processes in order to determine the \mathcal{P} omeron structure. First hard scattering results were obtained by the UA8 collaboration[10] using React. 1, and by the H1[11] and ZEUS[12] collaborations using ep interactions.

Factorization of \mathcal{P} omeron emission and interaction in the inclusive React. 1 is expressed by writing the single-diffractive differential cross section as a product of a \mathcal{P} omeron Flux Factor in the proton, $F_{\mathcal{P}/p}(t, \xi)$, and a proton- \mathcal{P} omeron total cross section.

$$\frac{d^2\sigma_{sd}}{d\xi dt} = F_{\mathcal{P}/p}(t, \xi) \cdot \sigma_{p\mathcal{P}}^{total}(s') \quad (2)$$

s' is the squared invariant mass of the X system and, to good approximation, is given by: $s' = \xi s$. The forms of $F_{\mathcal{P}/p}(t, \xi)$ and $\sigma_{p\mathcal{P}}^{total}$ in the context of Regge phenomenology are given below in Sect. 2.

Although there are many examples in the literature of the validity of factorization and Eq. 2, for example in Refs. [10–14], the total diffractive cross section prediction for React. 1 (the integral of the Regge version of Eq. 2 - see Sect. 2) is inconsistent with inelastic diffraction data and leads to a violation of unitarity near present collider energies. This problem deserves re-examination and confrontation with presently available diffractive data.

The rising total pp cross sections observed at the ISR in the early 1970s led to the conclusion[15, 16] that the effective \mathcal{P} omeron Regge trajectory intercept, $\alpha(0) = 1 + \epsilon$, was larger than unity⁵. The observation[20] that $\epsilon > 0$ violates the Froissart-Martin unitarity bound[21, 20] presents no difficulty at present and foreseeable collider energies. However, already at present collider energies, $\epsilon > 0$ creates problems for partial cross sections, and in particular for diffraction. This is easily seen by examining the dominant

⁴We use the symbol ξ for this variable in view of its simplicity and its increasing use in the literature.

⁵The fit result for the trajectory in Ref. [15] was $1.06 + 0.25t$; the latest refined fits[17, 18, 19] to the s -dependence of all total cross sections yield $\epsilon \sim 0.10$.

ξ -dependent Regge factor in Eq. 2 at small- ξ and small- t , which is included in the definition of $F_{\mathcal{P}/p}(t, \xi)$:

$$\frac{d^2\sigma_{sd}}{d\xi dt} \approx \xi^{1-2\alpha(0)} = \frac{1}{\xi^{1+2\epsilon}}, \quad (3)$$

Kinematically, ξ has a minimum value in React. 1, $\xi_{min} = s'_{min}/s$, which decreases with increasing energy, such that the rise in $F_{\mathcal{P}/p}(t, \xi)$ at small ξ becomes more and more pronounced. With $\epsilon = 0.10$, this leads to a rapidly increasing predicted total single diffractive cross section, σ_{sd}^{total} , with s , shown as the solid curve in Fig. 2. Of course, the observed σ_{sd}^{total} do not display this behavior, but rise much more modestly with s .

Nature avoids the violation of unitarity in inelastic diffraction with the addition of multi- \mathcal{P} omeron-exchange effects[22, 23, 24] (Regge cuts), described variously in the literature as screening, shadowing, absorption or damping. Eq. 2, traditionally used with the ϵ obtained from fitting total cross section data, does not take this into account.

In fact, it is expected[23] that multi- \mathcal{P} omeron-exchange effects increase with s , and that this should result in a decreasing effective ϵ . However, to the best of our knowledge, the correct effective ϵ values have never been directly extracted from hadronic data, although Schuler and Sjöstrand[25] have developed a model of hadronic diffractive cross sections in which they use $\epsilon = 0$ as a reasonable approximation. In γ^*p interactions at HERA, an Q^2 -dependent effective \mathcal{P} omeron intercept has been observed[26, 27], which is also believed to result from screening effects [28–31].

We recently demonstrated[32], using ISR and SPS data, that the unitarity-violating part of the predicted σ_{sd}^{total} is confined to the small- t , small- ξ domain. Since damping in this domain can be produced by simply decreasing the effective \mathcal{P} omeron intercept (see Eq. 3), in the present paper we use the measured inelastic diffraction cross sections to determine the effective ϵ values as a function of energy. The s -dependent effective \mathcal{P} omeron intercept is then smoothly connected to a relatively s -independent value of the trajectory[13] (~ 0.92) in the higher- $|t|$ region, 1.0–1.5 GeV 2 , to yield a new effective \mathcal{P} omeron trajectory for inelastic diffraction.

Sect. 2 summarizes the analysis by the UA8 collaboration[13], in which they fit Eq. 2 to ISR and SPS data; they obtain parametrizations of $F_{\mathcal{P}/p}(t, \xi)$ and $\sigma_{p\mathcal{P}}^{total}$ which embody features not previously known and specify the \mathcal{P} omeron trajectory at high- $|t|$. Sect. 3 shows how the effective \mathcal{P} omeron intercept depends on interaction energy in React. 1 and how predictions at $\sqrt{s} = 1800$ GeV agree with the CDF collaboration’s results[33]. The analysis in Sect. 4 yields a new \mathcal{P} omeron trajectory which depends on s only at low- $|t|$. Finally, Sect. 5 contains our conclusions and a discussion of some consequences.

2 UA8 Triple-Regge fits and the \mathcal{P} omeron trajectory at high- $|t|$

The UA8[13] collaboration analyzed data from their experiment at the CERN SPS-Collider ($\sqrt{s} = 630$ GeV) in the $|t|$ -range, 0.90–2.00 GeV 2 , and from the CHLM experiment at the CERN ISR[34] ($\sqrt{s} = 23$ –62 GeV) in the $|t|$ -range, 0.15–2.35 GeV 2 .

Eq. 2 was fit to the data, using the dominant two terms in the Mueller–Regge expansion[1, 2, 4], \mathcal{PPP} and \mathcal{PPR} (see Fig. 1), for the differential cross section of React. 1. These correspond, respectively, to \mathcal{P} omeron exchange and the exchange of other non-leading, $C=+$ \mathcal{R} eggeon trajectories (e.g., f_2) in the \mathcal{P} omeron–proton interaction,

$$\frac{d^2\sigma_{sd}}{d\xi dt} = [K F_1(t)^2 e^{bt} \xi^{1-2\alpha(t)}] \cdot \sigma_0[(s')^{\epsilon_1} + R(s')^{\epsilon_2}]. \quad (4)$$

Comparing with Eq. 2, the left-hand bracket is the \mathcal{P} omeron flux factor, $F_{\mathcal{P}/p}(t, \xi)$, and the right-hand bracket (together with the constant, σ_0) is the \mathcal{P} omeron–proton total cross section, $\sigma_{p\mathcal{P}}^{total}$. The exponents used, $\epsilon_1 = 0.10$, and $\epsilon_2 = -0.32$, correspond to those used in the description of real particle cross sections[17, 18]⁶.

In Eq. 4, $|F_1(t)|^2$ is the standard Donnachie–Landshoff[35] form–factor⁷ which is multiplied by a possible correction for high– $|t|$, e^{bt} . Thus, the product, $|F_1(t)|^2 e^{bt}$, carries the t –dependence of $G_{\mathcal{PPP}}(t)$ and $G_{\mathcal{PPR}}(t)$ in the Mueller–Regge expansion and is assumed to be the same in both. Physically, this means that the \mathcal{P} omeron has the same flux factor in the proton, independent of whether the \mathcal{P} omeron–proton interaction proceeds via \mathcal{P} omeron–exchange or \mathcal{R} eggeon–exchange. The products, $K\sigma_0 = G_{\mathcal{PPP}}(0)$, and $K\sigma_0 R = G_{\mathcal{PPR}}(0)$.

The \mathcal{P} omeron trajectory, $\alpha(t)$, was assumed to have the usual linear form with a quadratic term added to allow for a flattening of the trajectory at high– $|t|$, as required by the data:

$$\alpha(t) = 1.10 + 0.25t + \alpha''t^2 \quad (5)$$

Although we show in the present paper that the intercept decreases with s , fixing the intercept used in the UA8 fits at 1.10 is consistent with the data, since the only low– $|t|$ data used in the fit is from the ISR, where 1.10 is acceptable.

To avoid difficulties with differing experimental resolutions in the combined ISR–UA8 data sample, simultaneous fits of Eq. 4 were made to data in the range $0.03 < \xi < 0.04$ and $|t| < 2.25$ GeV² with no background assumed; then fits were made to the entire region, $0.03 < \xi < 0.10$, including a background term of the form $Ae^{ct}\xi^1$. All fits were self–consistent. The fitted values[13, 32] of the four free parameters in Eq. 4:

$$\begin{aligned} K\sigma_0 &= 0.72 \pm 0.10 \quad \text{mb GeV}^{-2} \\ \alpha'' &= 0.079 \pm 0.012 \quad \text{GeV}^{-4} \\ b &= 1.08 \pm 0.20 \quad \text{GeV}^{-2} \\ R &= 4.0 \pm 0.6 \end{aligned}$$

The fitted \mathcal{P} omeron trajectory, Eq. 5 with $\alpha'' = 0.08$, is shown as the shaded band in Fig. 3. The band edges correspond to $\pm 1\sigma$ error limits on α'' .

Independent confirmation of the $\alpha(t)$ values at high– $|t|$ seen in Fig. 3 was obtained by fitting (resolution–smeared) Eq. 4 to the ξ –dependence of the UA8 data at fixed– t in the

⁶The UA8 fitted value of R is similar to what is found in the fits to real particle cross sections.

⁷ $F_1(t) = \frac{4m_p^2 - 2.8t}{4m_p^2 - t} \cdot \frac{1}{(1-t/0.71)^2}$

different ξ -region, $\xi < 0.03$, where non-Pomeron-exchange background could be ignored. Although, in Eq. 4, the dominant ξ -dependence is in $F_{\mathcal{P}/p}(t, \xi)$ and has the form $\xi^{1-2\alpha(t)}$, there are the additional (weaker) $(s')^\epsilon \sim \xi^\epsilon$ dependences in the \mathcal{PPP} and \mathcal{PPR} terms of $\sigma_{p\mathcal{P}}^{total}$, both of which must be included in the fit. Because the (\mathcal{PPR}) term is more sharply peaked at small values of ξ than is the \mathcal{PPP} term, leaving it out of the fit⁸ causes a systematic upward shift in the resultant $\alpha(t)$. We come back to this point in Sect. 3.1 when we discuss results from the CDF experiment[33].

The solid points in Fig. 3 show the fitted values[13] of $\alpha(t)$ at four t -values, when both \mathcal{PPP} and \mathcal{PPR} terms in Eq. 4 are used in the fit (with $R = 4.0$). The solid points and the band in the figure are in good agreement. The two different, but self-consistent, fits to the data in the high- $|t|$ region give confidence in the value of the overall normalization constant, $K\sigma_0$, and in the t -dependence, $|F_1(t)|^2 e^{bt}$.

Table 1 summarizes the two types of fits performed by the UA8 collaboration in determining $\alpha(t)$ at high t , and shows which data sets were used in each. In Sect. 4, a third type of fit is described which also yields essentially the same results at high- $|t|$.

3 An s -dependent effective intercept

As explained above, a σ_{sd}^{total} prediction depends sensitively on the value of ϵ which is used. For each of the ISR, SPS and Tevatron points in Fig. 2, we have therefore found the ϵ which yields the measured σ_{sd}^{total} . Eq. 4 is integrated over $\xi < 0.05$ and all t , with the following assumptions:

1. The UA8 parameter values given in Sect. 2 are used for $K\sigma_0$ and R .
2. We set $b = 0$ and $\alpha'' = 0$, which is a reasonable approximation because they contribute little in the small- $|t|$ region which dominates the cross section.
3. We only vary the ϵ which appears in the Flux Factor, $F_{\mathcal{P}/p}(t, \xi)$. Because the fitted R parameter (see above) is similar to that found fitting real particle total cross sections and σ_{sd}^{total} is dominated by small mass in Eq. 4, we fix $\epsilon_1 = 0.10$ and $\epsilon_2 = -0.32$.

Fig. 4 shows the resulting ϵ values vs. s ; their errors only reflect the measurement errors in the σ_{sd}^{total} points. Starting in the ISR region, the points display a downward trend, reaching around 0.01–0.02 at the highest Tevatron energy. Since, a priori, we do not know what value of the slope, α' , to use, and it may be flatter at small values in order to connect with the UA8 high- $|t|$ $\alpha(t)$ points shown in Fig. 3, we show the calculated ϵ at the two highest energies for two different values of α' . There is no change in the essential feature of the plot.

⁸Note that this means assuming $R = 0$, which is in blatant disagreement with the value, $R = 4.0$ quoted above.

3.1 Predictions for the Tevatron

A small value of the intercept in the Flux Factor of Eq. 4 has the consequence that the shape of the observed ξ –distribution should be flatter. For example, Fig. 5 shows Eq. 4 plotted vs. ξ at $\sqrt{s} = 1800$ GeV and small momentum transfer, $|t| = 0.05$ GeV², for different values of ϵ ($\alpha' = 0.25$ is used for these curves). The flattening of the curves is evident as ϵ decreases from 0.1 to 0.0; the magnitude of the predicted cross section also decreases.

We now compare the predictions in Fig. 5 with the results of the CDF experiment[33] at $\sqrt{s} = 1800$ GeV, which they give only in the form of a function fitted to their corrected differential cross section. Their function is similar to our Eq. 4, except for three differences. They assume a linear \mathcal{P} omeron trajectory and an exponential t –dependence, both of which are valid because their data are only at low– $|t|$. More significantly, however, they ignore the \mathcal{PPR} term in σ_{sd}^{total} . However, it was pointed out[32] that use of the wrong function leads to an artificial separation of their fitted “signal” and “background” and an overestimate of the background. Moreover, as shown by UA8[13], this also leads to an overestimate of $\alpha(t)$. Although Fig. 17 in CDF’s Ref. [33] demonstrates how ϵ would decrease with an increasing fraction of \mathcal{PPR} contribution in σ_{sd}^{total} , without a multi–energy fit of the type done by UA8, they were not able to quote a specific value of ϵ with both terms taken into account⁹.

We estimate the true effective ϵ of the CDF data by taking their fitted function (“signal” plus “background”) as a good representation of their corrected differential cross section, and comparing it with predictions using the UA8 parametrization for different values of ϵ . The solid curve in Fig. 5 shows the ξ –dependence of the CDF function, and is seen to lie between the predictions for $\epsilon = 0.0$ and 0.05 , agreeing in both absolute magnitude and shape to an effective ϵ about 0.03. The small discrepancy between this value and the one shown in Fig. 4 can be due to a small mismatch between the t –dependence used in our Eq. 4 and the CDF function, as well as in the value of $\alpha' = 0.25$ used in the predictions.

4 The \mathcal{P} omeron trajectory

Having established the need for a new effective \mathcal{P} omeron intercept, we now examine how it may be connected to the high– $|t|$ α points shown in Fig. 3. From the results in Sect. 3 at low– $|t|$, we have an effective trajectory and intercept which reflects multi– \mathcal{P} omeron–exchange effects. However, at high– $|t|$ the trajectory shows no signs of an s –dependence, since the triple–Regge formalism describes the data between ISR and SPS with no apparent need of damping[32].

In order to determine the full \mathcal{P} omeron trajectory, we resort to a somewhat unorthodox procedure. We rely on the validity of the t –dependence, $|F_1(t)|^2 e^{bt}$ in $F_{\mathcal{P}/p}(t, \xi)$, and fit $\alpha(t)$, such that the $\xi < 0.05$ integral of Eq. 4 agrees with the observed $d\sigma_{sd}/dt$.

⁹CDF quoted a value, $\epsilon = 0.103 \pm 0.017$, corresponding to zero contribution from \mathcal{PPR} .

There is only one set of $d\sigma_{sd}/dt$ data above ISR energies which covers the complete $|t|$ range from 0–2 GeV². Fig. 6 shows the measurements at the SPS-Collider by the UA4 collaboration[36, 37] (open points) and by the UA8 collaboration[13] (solid points). The UA4 data cover most of the t –range because they come from independent high– β and low– β runs at the SPS. The UA8 data only cover the high– $|t|$ part of the range, but they are in good agreement with the UA4 points where they overlap¹⁰. Although the poor ξ resolution of the low– β run precludes use of the data for fits to the ξ –dependence, the $d\sigma_{sd}/dt$ distribution is hardly influenced.

Thus we fit the $\xi < 0.05$ integrated version of Eq. 4 to the $d\sigma_{sd}/dt$ points in Fig. 6 assuming, in turn, two simple parametrizations of $\alpha(t)$. In the fits, $K\sigma_0$, b and R are fixed at the UA8 values given above. The two resulting trajectories are shown in Fig. 3. They are very similar. The solid curve is quadratic, $\alpha(t) = \alpha_0 + \alpha' t + \alpha'' t^2$, with three free parameters (1.035 ± 0.001 , 0.165 ± 0.002 GeV^{–2} and 0.059 ± 0.001 GeV^{–4}, respectively). The dashed trajectory in Fig. 3, consisting of two straight lines, also has three free parameters, the slope and intercept and the t value at which the trajectory continues horizontally to larger– $|t|$ values (1.033 ± 0.001 , 0.134 ± 0.003 GeV^{–2} and 0.80 ± 0.02 GeV², respectively). Since the t integral of $d\sigma_{sd}/dt$ is σ_{sd}^{total} , the trajectory at low– $|t|$ reflects the same result discussed in Sect. 3. The third entry in Table 1 summarizes the method and data used for these fits. It is remarkable that the fitted trajectories agree rather well with the solid points and shaded band (at high– $|t|$) in Fig. 3, which were independently obtained.

Fig. 6 shows the resulting fits to $d\sigma_{sd}/dt$ for the two cases, with χ^2/DF values of 4.2 (solid curve) and 2.0 (dashed curve)¹¹. Our approximate trajectories thus yield acceptable fits to the observed $d\sigma_{sd}/dt$ at SPS energies for the first time.

5 Discussion

In the present Letter, using the results in Refs. [13, 32], it is demonstrated that the triple Regge formula (with both \mathcal{PPP} and \mathcal{PPR} terms) describes all available inclusive single–diffractive data from ISR to Tevatron, provided that the effective \mathcal{P} omeron Regge trajectory intercept, $\alpha(0)$, is s –dependent and decreases from a value, 1.10, at low energies to a value about 1.03 at the SPS-Collider. This result, when combined with a (confirmed) knowledge of the trajectory, $\alpha(t) \sim 0.92 – 0.95$ in the range, $1.0 < |t| < 1.5$ GeV², specifies a new \mathcal{P} omeron trajectory in inelastic diffraction. Its low– t behavior is in disagreement with the “traditional” soft \mathcal{P} omeron trajectory, obtained from fits to the energy dependence of hadronic total cross sections. The inverse dependence of ϵ on the contribution of multi– \mathcal{P} omeron–exchange is similar to what is found in in γ^*p interactions[26, 27] at HERA.

We find it remarkable that, despite the presence of multi– \mathcal{P} omeron–exchange contributions, Eq. 2 and the factorization of \mathcal{P} omeron emission and interaction retain a high

¹⁰We ignore the small difference between the two \sqrt{s} values, 546 and 630 GeV.

¹¹An improved fit could certainly be obtained with a higher order function.

degree of validity. This suggests that multi-Pomeron-exchange behaves in an approximately factorizable way[38].

It is perhaps relevant to note that a recent UA8 analysis[39] of their double-Pomeron-exchange data shows that there is a pronounced enhancement of the Pomeron-Pomeron cross section in the few-GeV mass region, with about a factor of ten larger cross section than is expected from factorization. It is evident that such strong Pomeron-Pomeron interactions can have a significant, and perhaps simplifying, impact on the nature of the effective Pomeron exchange. We also note that damping of small- ξ (or, via Eq. 3 with a smaller effective ϵ) leads to an larger average ξ of the emitted Pomeron system. Heuristically speaking, this may be related to the emission of a multi-Pomeron system.

The apparent absence of damping in the high- $|t|$ data[32] suggests that the trajectory is perturbative in this domain. It is therefore desirable that high- $|t|$ measurements be made at the highest Tevatron energy in order to confirm this view. If this is indeed a perturbative domain, it will be very interesting to note if the same trajectory is active in high- Q^2 diffractive γ^*p interactions. In this connection, the H1 collaboration[40] has recently reported results on J/Ψ photoproduction from which an α value around unity (at the 1σ lower bound) is reported for $|t| > 1$ GeV 2 .

Currently available data do not permit the measurement of the effective $\alpha(t)$ in the moderate $|t|$ region, say between 0.2 and 1.0 GeV 2 . In order to understand the precise shape of the trajectory in this domain, new data will be required at several energies. Fits of the type carried out by the UA8 collaboration, namely simultaneously fitting the ξ -dependence of the differential cross section at several energies in the small- ξ region and at fixed t values, have the advantage that no assumption need be made about the functional dependence on t and non-Pomeron-exchange background can be ignored.

One consequence of our results is that predictions of jet production in hard diffraction at the Tevatron should use $\epsilon = 0.03$. We note that, numerically, this is approximately equivalent to Goulianos' "renormalization" procedure[41] in predicting total cross sections, but has the advantage that ξ and t dependences are now correctly predicted.

A theoretical challenge for the future is to calculate multi-Pomeron-exchange effects, taking into account a large low-mass Pomeron-Pomeron interaction, as well as the effective Pomeron trajectory. The results of such calculations should also preserve the high degree of factorization exhibited by the data.

Acknowledgements

We wish to thank John Dainton, Alexei Kaidalov and Yuri Maor for helpful discussions. We also wish to thank the CERN laboratory, where this work was done, for their long hospitality.

Results in Fig. 3	Type of fit	Cross section used ?	SPS		ISR	
			low- $ t $	high- $ t $	low- $ t $	high- $ t $
Points	Shape of ξ distribution at fixed- t ($\xi < 0.03$)	NO		✓		
Shaded Band	Fit $d^2\sigma_{sd}/d\xi dt$ ($0.03 < \xi < 0.10$)	YES		✓	✓	✓
Curves	Fit $d\sigma_{sd}/dt$	YES	✓	✓		

Table 1: The three types of fits which have yielded the Pomeron Regge trajectory in the high- $|t|$ domain, 1.0-1.5 GeV 2 , shown in Fig. 3.

References

- [1] A.H. Mueller, Phys. Rev. D 2 (1970) 2963; D 4 (1971) 150.
- [2] S.D. Ellis and A.I. Sanda, Phys. Rev. D 6 (1972) 1347.
- [3] A.B. Kaidalov et al., JETP Lett. 17 (1973) 440;
A. Capella, Phys. Rev. D 8 (1973) 2047;
- [4] R.D. Field and G.C. Fox, Nucl. Phys. B 80 (1974) 367;
D.P. Roy and R.G. Roberts, Nucl. Phys. B 77 (1974) 240;
- [5] see: P.D.B. Collins, “An Introduction to Regge Theory & High Energy Physics”, Cambridge University Press (1977), and references therein.
- [6] A.B. Kaidalov, Phys. Reports 50 (1979) 157.
- [7] G. Ingelman and P.E. Schlein, Phys. Lett. B 152 (1985) 256.
- [8] E.L. Berger, J.C. Collins, D.E. Soper and G. Sterman, Nucl. Phys. B 286 (1987) 704.
- [9] A. Donnachie & P.V. Landshoff, Phys. Lett. 191 (1987) 309; Nucl. Phys. B 303 (1988) 634; Phys. Lett. B 285 (1992) 172.
- [10] R. Bonino et al. (UA8 Collaboration), Phys. Lett. B 211 (1988) 239;
A. Brandt et al. (UA8 Collaboration), Phys. Lett. B 297 (1992) 417;
A. Brandt et al. (UA8 Collaboration), Phys. Lett. B 421 (1998) 395.

- [11] T. Ahmed et al. (H1 Collaboration), Nucl. Phys. B 429 (1994) 477;
 C. Adloff et al. (H1 Collaboration), Zeit. f. Phys. C 76 (1997) 613;
 C. Adloff et al. (H1 Collaboration), Europhys. Journal C 6 (1999) 421.
- [12] M. Derrick et al. (ZEUS Collaboration), Phys. Lett. B 315 (1993) 481;
 J. Breitweg et al. (ZEUS Collaboration), Eur. Phys. J. C1 (1998) 81;
 J. Breitweg et al. (ZEUS Collaboration), Eur. Phys. J. C6(1999) 43.
- [13] A. Brandt et al. (UA8 Collaboration), Nucl. Phys. B 514 (1998) 3.
- [14] R.L. Cool et al., Phys. Rev. Lett. 47 (1981) 701.
- [15] P.D.P. Collins, F.D. Gault and A. Martin, Phys. Lett. B 47 (1973) 171; Nucl. Phys. B 80 (1974) 135.
- [16] A. Capella and J. Kaplan, Phys. Lett. B 52 (1974) 448.
- [17] J.R. Cudell, K. Kang and S.K. Kim, Phys. Lett. B395 (1997) 311; see also: Cudell et al., “High energy forward scattering and the \mathcal{P} omeron: simple pole vs. unitarized models”, hep-ph/9908218.
- [18] R.J.M. Covolan, J. Montanha & K. Goulian, Phys. Lett. B389 (1996) 176.
- [19] A. Donnachie & P.V. Landshoff, Phys. Lett. B 296 (1992) 227.
- [20] A. Martin, Phys. Rev. 129 (1963) 1432.
- [21] M. Froissart, Phys. Rev 123 (1961) 1053.
- [22] A. Capella, J. Kaplan and J. Tran Thanh Van, Nucl. Phys. B 105 (1976) 333.
- [23] A.B. Kaidalov. L.A. Ponomarev and K.A. Ter-Martirosyan, Sov. Journal of Nucl. Phys. 44 (1986) 468.
- [24] E. Gotsman, E.M. Levin and U. Maor, Phys. Lett. B 309 (1993); Phys. Rev. D 49 (1994) 4321.
- [25] G.A. Schuler and T. Sjöstrand, Phys. Rev. D 49 (1994) 2257.
- [26] S. Aid et al. (H1 Collaboration), Nucl. Phys. B 470 (1996) 3; “Precision measurement of the inclusive deep inelastic ep scattering cross section at low Q^2 at HERA”, Abstract 534, ICHEP-98 (Vancouver, July 1998).
- [27] J. Breitweg et al. (Zeus Collaboration), Eur. Phys. Journal C 7 (1999) 609.
- [28] A. Capella, A. Kaidalov, C. Merino and J. Tran Thanh Van, Phys. Lett B 337 (1994) 358; Phys. Lett B 343 (1995) 403.
- [29] M. Bertini, M. Giffon and E. Predazzi, Phys. Lett. B 349 (1995) 561.

- [30] E. Gotsman, E.M. Levin and U. Maor, Eur. Phys. J. C 5 (1998) 303.
- [31] H. Abramowicz, E.M. Levin, A. Levy and U. Maor, Phys. Lett. B 269 (1991) 465; H. Abramowicz and A. Levy, “The ALLM parametrization of $\sigma_{tot}(\gamma^*p)$, an update”, DESY 97-251.
- [32] S. Erhan and P. Schlein, Phys. Lett. B 427 (1998) 389; due to a publisher’s misprint of Figs. 4 and 7, they were reprinted correctly in: Phys. Lett. B 445 (1999) 455.
- [33] F. Abe et al. (CDF Collaboration), Phys. Rev. D 50 (1994) 5535.
- [34] M.G. Albrow et al. (CHLM Collaboration), Nucl. Phys. B54 (1973) 6; Nucl. Phys. B72 (1974) 376.
- [35] A. Donnachie & P.V. Landshoff, Nucl. Phys. B231 (1984) 189; Nucl. Phys. B267 (1986) 690.
- [36] M. Bozzo et al. (UA4 Collaboration), Phys. Lett. B136 (1984) 217.
- [37] D. Bernard et al. (UA4 Collaboration), Phys. Lett. B186 (1987) 227.
- [38] J. Pumplin and G.L. Kane, Phys. Rev. Lett. 32 (1974) 963.
- [39] “The \mathcal{P} omeron– \mathcal{P} omeron Total Cross Section”: S. Erhan (UA8 Collaboration), Proceedings of 4th Workshop on Small- x and Diffractive Physics (Fermilab, 17-20 September, 1998) 385; also, to be published (1999)
- [40] H1 Collaboration, “Diffractive J/Ψ Photoproduction”, Contribution to International Europhysics Conference on High Energy Physics HEP99 (Tampere, Finland, July 1999); Abstract: 157aj; see: <http://www-h1.desy.de/publications/>
- [41] K. Goulianos, Phys. Lett. B 358 (1995) 379; B 363 (1995) 268.

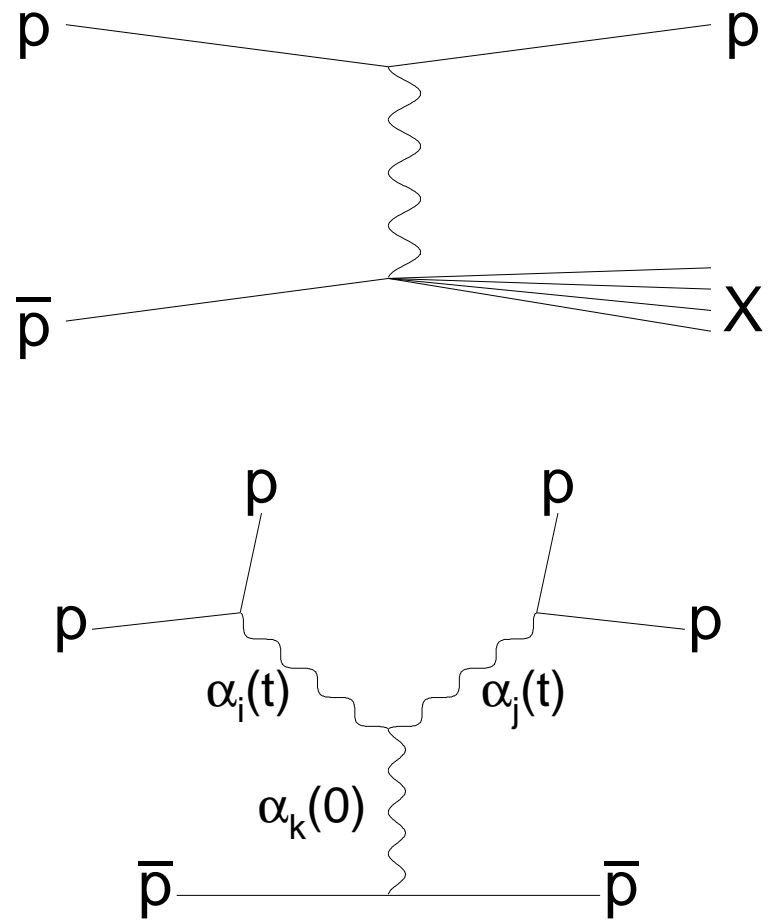


Figure 1: Upper: The diffractive $\bar{p}p$ process. The exchanged \mathcal{P} omeron has a momentum transfer, t , and momentum fraction, $\xi \equiv x_{\mathcal{P}} = 1 - x_p$, of the incident proton. The squared invariant mass of the X system is $M_X^2 = s' = \xi s$. Lower: The triple-Regge version of the upper process.

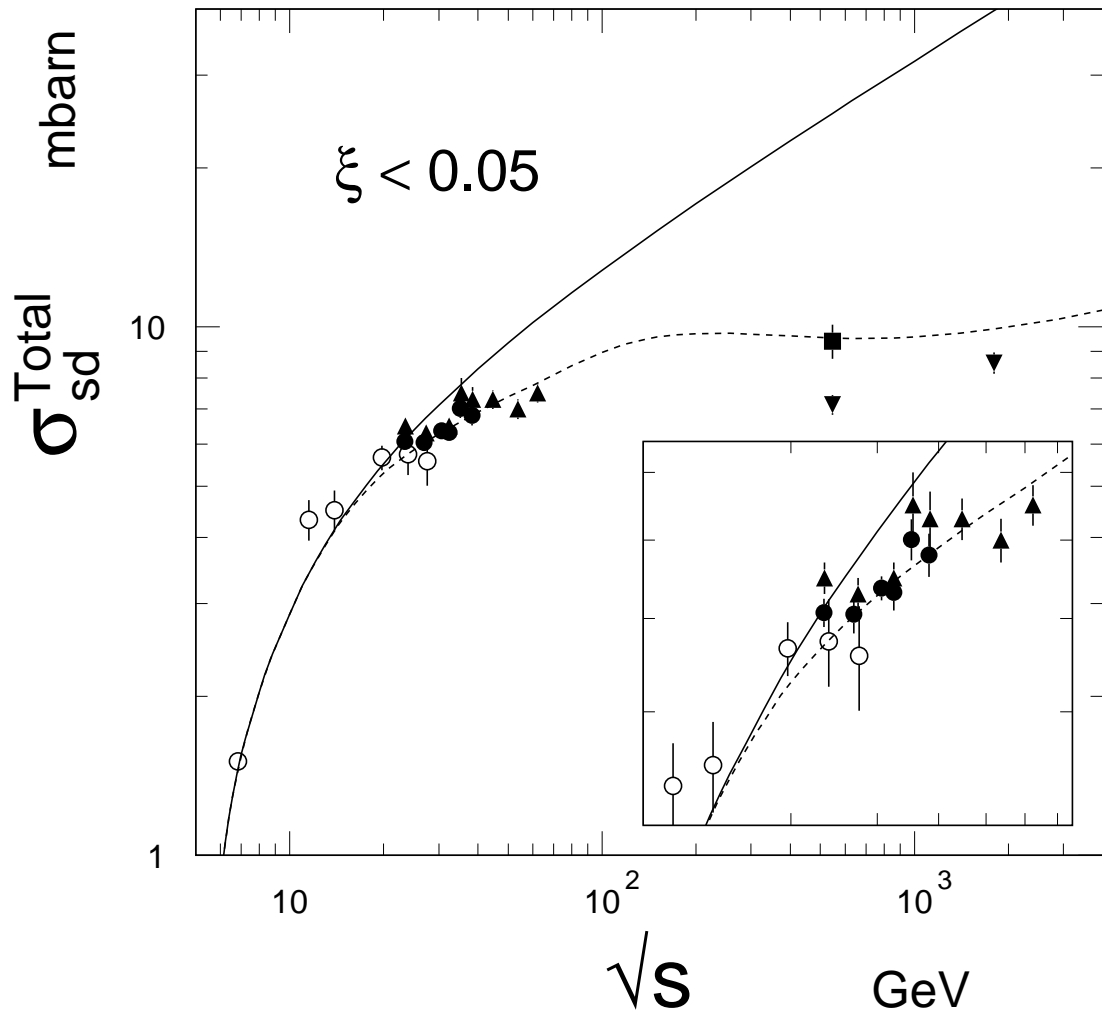


Figure 2: Measured total single diffractive cross section for $\xi < 0.05$ in pp or $p\bar{p}$ interactions vs. \sqrt{s} . A factor of two is included to account for both hemispheres (see the experiment references in Ref. [32]). The insert is a blow-up of the ISR energy range. The solid curve is the UA8 Triple-Regge prediction; the dashed curve shows the consequence of multiplying it by a “toy” damping factor[32].

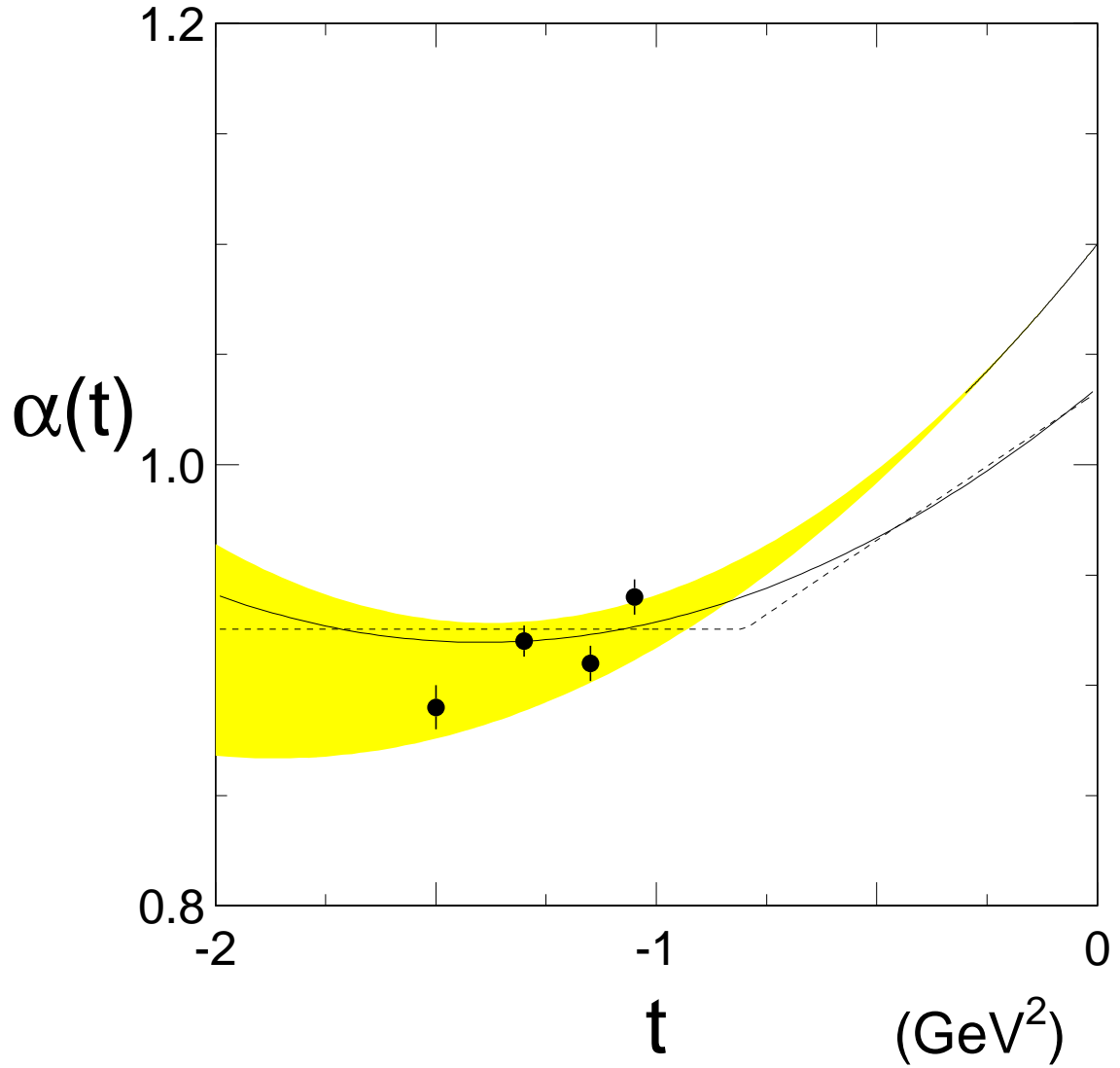


Figure 3: The effective \mathcal{P} omeron Regge trajectories at ISR and SPS. Solid points[13] are fits to the SPS data with $\xi < 0.03$ at fixed t . The shaded band[13] ($\alpha(t) = 1.10 + 0.25t + \alpha''t^2$ with $\alpha'' = 0.08$) results from a simultaneous fit to all ISR/SPS data in the range $0.03 < \xi < 0.10$ and $\sqrt{s} = 23 - 630$ GeV, but included only low- $|t|$ data at the ISR energies (see Table 1). The solid and dashed curves correspond to the new fits to the SPS $d\sigma_{sd}/dt$ with $\xi < 0.05$ as described in the text.

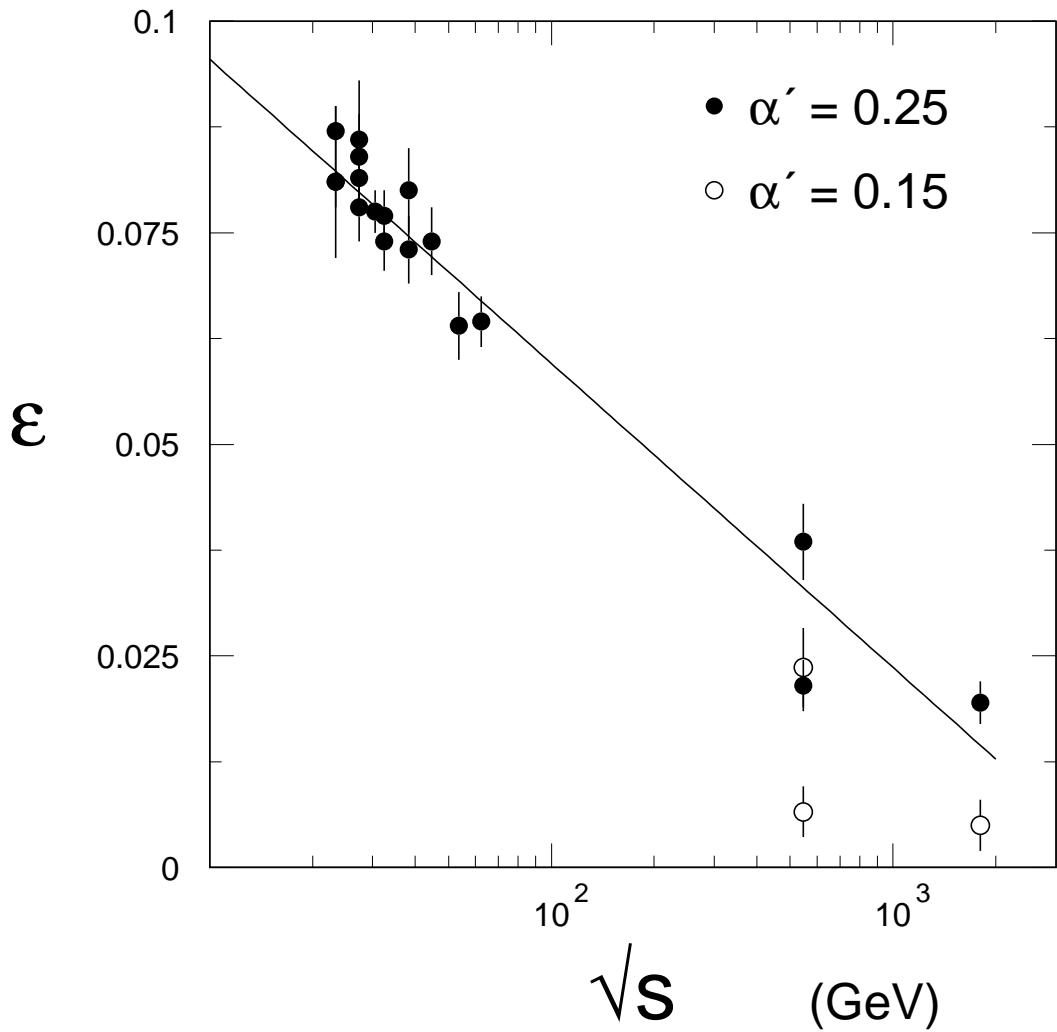


Figure 4: Calculated effective ϵ values (approximate) vs. s , which are required to make the predicted σ_{sd}^{total} values in Fig. 2 agree with the various measured values. The solid points assume $\alpha' = 0.25$. The highest energy points are also shown for $\alpha' = 0.15$ (open circles). The line is a fit to the solid points to emphasize the trend.

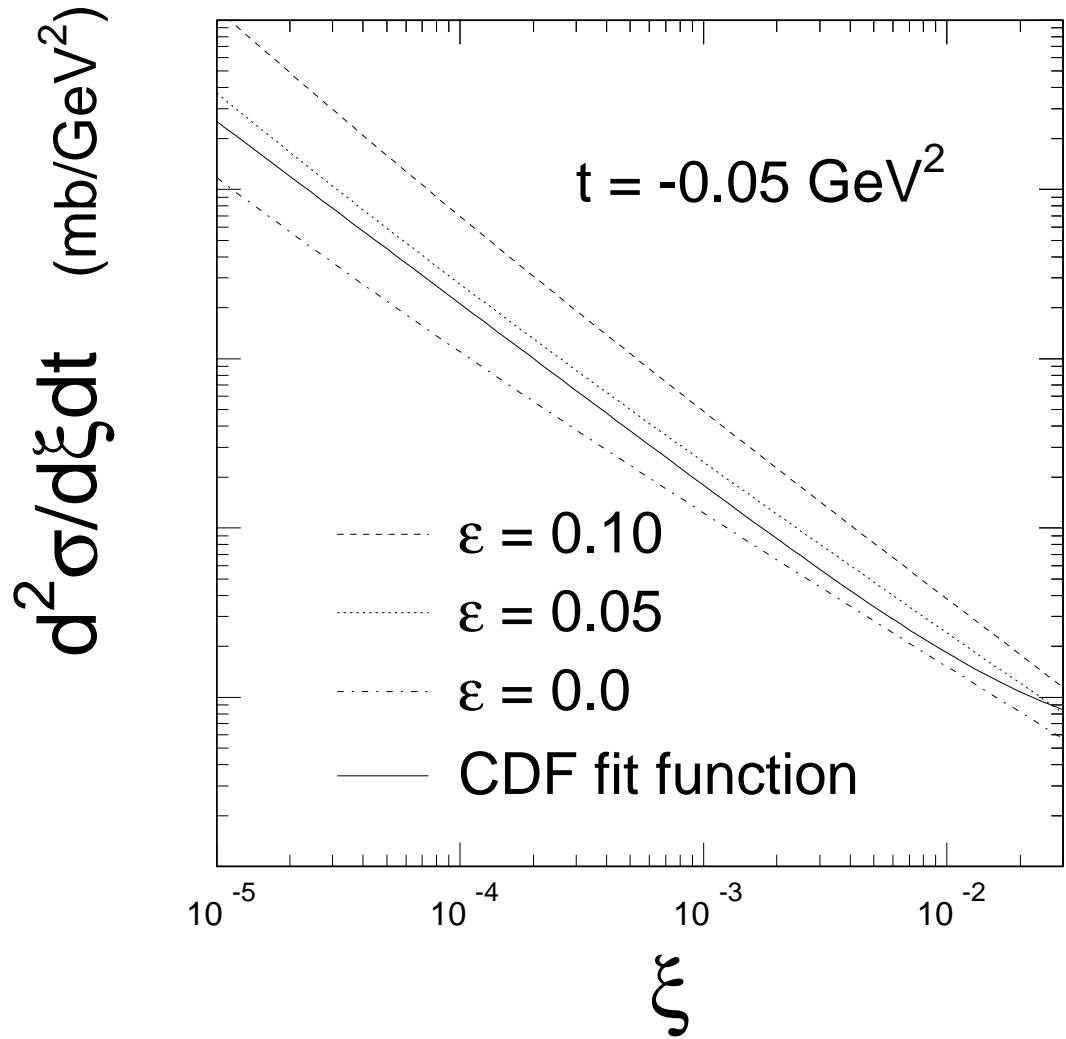


Figure 5: The CDF parametrization of their single diffractive differential cross section[33] (solid curve) vs. ξ at $|t| = 0.05 \text{ GeV}^2$ and $\sqrt{s} = 1800 \text{ GeV}$. As discussed in the text, predicted distributions using Eq. 4 and the UA8 fitted parameters are evaluated at three values of effective ϵ in $F_{P/p}(t, \xi)$ and plotted as dashed, dotted and dash-dotted curves.

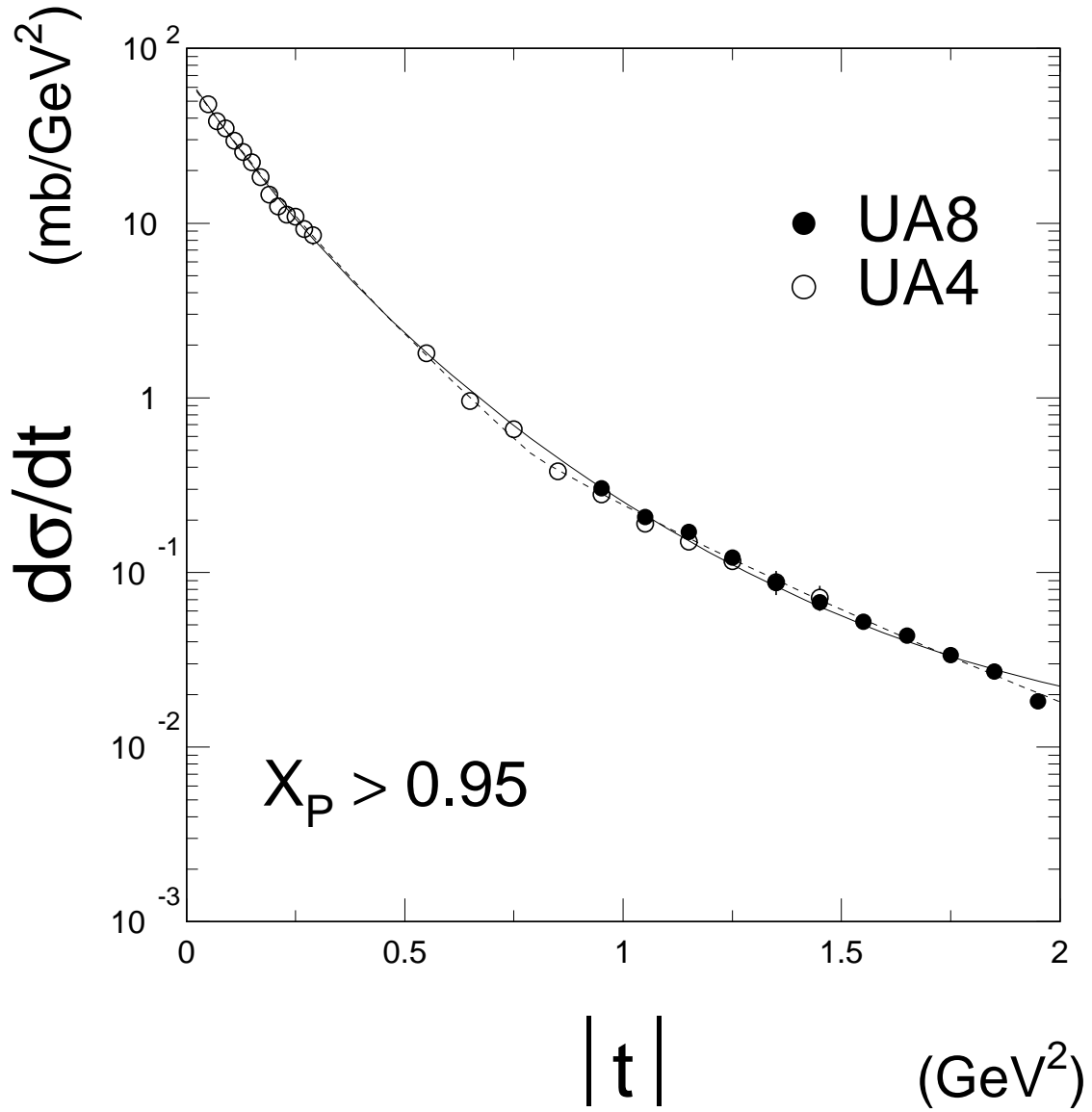


Figure 6: Inclusive differential cross sections for protons in React. 1 for $x_p > 0.95$, from experiments UA4[36, 37] with $\sqrt{s} = 546$ GeV and UA8[13] with $\sqrt{s} = 630$ GeV. The cross sections shown are for both p and \bar{p} excitation; the integral is $\sigma_{sd}^{total} = 9.4 \pm 0.7$ mb. The solid and dashed curves are fits corresponding to the solid and dashed \mathcal{P} omeron trajectories shown in Fig. 3 and described in the text.